Studies of multichannel rotational predissociation of Ar–H2 van der Waals molecule by the complexcoordinate coupledchannel formalism

ShihI Chu and Krishna K. Datta

Citation: The Journal of Chemical Physics **76**, 5307 (1982); doi: 10.1063/1.442929
View online: http://dx.doi.org/10.1063/1.442929
View Table of Contents: http://scitation.aip.org/content/aip/journal/jcp/76/11?ver=pdfcov
Published by the AIP Publishing

Studies of multichannel rotational predissociation of Ar–H_2 van der Waals molecule by the complex-coordinate coupled-channel formalism

Shih-I Chu[a] and Krishna K. Datta

Department of Chemistry, University of Kansas, Lawrence, Kansas 66045
(Received 23 June 1981; accepted 3 February 1982)

The complex-coordinate coupled-channel (CCCC) formalism previously developed [J. Chem. Phys. 72, 4772 (1980)] is applied to the accurate determination of the level widths (lifetimes) and energies of rotationally predissociating metastable Ar···H_2 van der Waals molecules. Calculations are performed using several realistic anisotropic potentials obtained recently by experiments, including Lennard-Jones (LJ), Buckingham–Corner (BC) type potentials, as well as the semiempirical potential of Tang–Toennies (TT). New numerical methods are introduced here to deal with the complex rotations of piecewise inhomogeneous potentials such as those of BC and TT. It is found that the CCCC method is capable of providing reliable results for any given potential surface. Furthermore, the CCCC results are sensitive to the potential surfaces used. For example, the linewidths predicted for different LJ potential surfaces considered here vary by a factor as large as 4. However, the agreement among more recent potentials, namely, the BC potential of Zandee and Reuss and that of Le Roy and Carley as well as the potential of Tang and Toennies, is much closer: the resonance energies agree to within 1 cm^{-1} and the linewidths to within 30%.

I. INTRODUCTION

Recently accurate determination of anisotropic intermolecular potentials between atoms and molecules is becoming possible due to the rapid development of the spectroscopy of van der Waals molecules,[1] the molecular beam measurements of orientation dependence of total cross sections for polarized molecules,[2,3] and the detailed theoretical analysis of pressure-induced infrared spectra.[4,5] Reliable potential surfaces (both isotropic and anisotropic) for several systems, particularly the rare gas–H_2 systems, are now available. In this paper we are concerned with the accurate determination of the resonance energies and widths (lifetimes) of metastable states of van der Waals complexes based on the realistic potential surfaces recently obtained from experiments. Such data, besides providing useful additional information on well depths and anisotropy of the intermolecular interactions, is important to the elucidation of the general features of bond breaking processes in chemical systems where the predissociation occurs by converting the internal vibration–rotation energies of the complexes into relative kinetic energies of the fragments. In addition, a knowledge of the lifetimes of such levels is relevant to the detectability of the complexes by the supersonic beam experiments and to the feasibility of isotope separation using the technique of photoinduced predissociation of selectively excited van der Waals molecules.[6]

Previous theoretical works of this problem have been summarized by Grabenstetter and Le Roy,[7] and Beswick and Requena.[8] Recently, one of the present authors[9] has proposed a *complex-coordinate coupled-channel formalism* employing only L^2 (square-integrable)-basis functions and the use of complex coordinate transformation.[10,14] Besides its practical simplicity, in that only bound state functions are involved and no asymptotic boundary conditions need to be enforced, the method is also readily extendable to many-channel problems involving multiple coupling continua.[24] We note that related approaches along this line have also recently appeared in the literature.[11]

In the present work we focus on the application of the complex-coordinate coupled-channel formalism[9] to the rotational predissociation of Ar–H_2 van der Waals molecules. In Sec. II, we discuss the model Hamiltonian used for the Ar–H_2 van der Waals complex. The complex-coordinate coupled-channel formalism is briefly sketched in Sec. III. In Sec. IV, the method is applied to several Ar–H_2 potential surfaces recently obtained by experiments, including Lennard-Jones (LJ) and Buckingham–Corner (BC) type potentials, as well as the semiempirical potential of Tang–Toennies (TT). *New* numerical methods are introduced here to deal with the complex rotation of *inhomogeneous piecewise* potentials such as those of BC and TT. Finally, we present the detailed converged results for the various Ar–H_2 surfaces in Sec. V.

II. THE MODEL HAMILTONIAN FOR Ar-H_2 VAN DER WAALS COMPLEX

The system under consideration consists of a diatomic rigid rotor H_2 with orientation $\hat{r}$ and an Ar atom with position R relative to the center of mass of the diatom. The Hamiltonian for the Ar–H_2 complex, within the Born–Oppenheimer approximation, can be represented by[5,7]

$$H(R,\theta)=\frac{1}{2\mu}\left[-\hbar^2\frac{\partial^2}{\partial R^2}+\frac{\mathbf{l}^2(\hat{R})}{R^2}\right]+B_{\rm rot}\,\mathbf{j}^2(\hat{r})+V(R,\theta)\,. \tag{2.1}$$

In this equation, μ = reduced mass of Ar–H_2, $\cos\theta = \hat{r}\cdot\hat{R}$, $B_{\rm rot}$ = rotational constant of H_2 (= 60.853 cm^{-1}),[34] $\mathbf{j}$ = rotational angular momentum of H_2, $\mathbf{l}$ = orbital angular momentum of H_2 and Ar about each other, and $V(R,\theta)$ = interaction potential of Ar and H_2. For the (weakly anisotropic) Ar–H_2 system, the interaction potential can

[a] Alfred P. Sloan Foundation Fellow.

 0021-9606/82/115307-14$02.10

be satisfactorily described by a two-term Legendre expansion[3-5]:

$$V(R,\theta) = V_0(R) + V_2(R) P_2(\cos\theta) , \tag{2.2}$$

where $V_0(R)$ describes the radial dependence of the spherically symmetric (isotropic) part and $V_2(R)$ that of the anisotropic part. Accurate determination of V_0 and V_2 has been achieved recently due to both experimental and theoretical efforts.[3-5,21] In particular, V_0 can now be considered to be known experimentally in the well region to better than about 1%. The precision of $V_2(R)$, in general, depends to some extent on the assumed potential model for V_0 and its parameter. Among the most sensitive and accurate measurements of potential anisotropies to date are those provided by the experiments of Zandee and Reuss,[3] and of Waaijer.[21] Tang and Toennies[12] have also recently proposed a simple semiempirical theory of the van der Waals potential which appears to provide accurate anisotropic potentials for rare-gas-H_2 systems. A detailed discussion on the potential models used in this study will be postponed until Sec. IV.

The predissociation resonances associated with the atom-rigid rotor diatom complex can be qualitatively understood as follows. During a low (subexcitation) energy molecular collision, the kinetic energy of relative motion can be converted into internal (rotational) excitation and the attractive mutual interaction between the excited molecules can then lead to temporary formation of a metastable van der Waals complex. The width of the resonance is associated with the dissociation of the van der Waals molecule which occurs when the internal energy is reconverted into the relative translational energy along the atom–diatom van der Waals bond and the fragments separate. In the present case of the atom-rigid rotor diatom, the predissociation width is induced by the potential anisotropy. In the next section we outline a method for determining the energies and widths of such metastable levels.

III. COMPLEX-COORDINATE COUPLED-CHANNEL FORMALISM FOR ROTATIONAL PREDISSOCIATION OF VAN DER WAALS MOLECULES

As details of the complex-coordinate coupled-channel formalism have been discussed in the previous paper,[9] only an outline of the method will be presented here to serve the definition of notations.

In the total angular momentum (J, M) representation, $\mathbf{J} = \mathbf{l} + \mathbf{j}$, a convenient angular basis for wave function expansion is the total angular momentum eigenfunction defined by[13]

$$\mathcal{Y}^M_{Jlj}(\hat{R},\hat{r}) = \sum_{m_l}\sum_{m_j} (lj m_l m_j | ljJM)\, Y_{lm_l}(\hat{R}) Y_{jm_j}(\hat{r}) , \tag{3.1}$$

where $(\ldots|\ldots)$ is the Clebsch-Gordan coefficient and Y_{km_k} are the spherical harmonics. It is expedient to define a scheme[5] for labeling of the eigenstates of the complex uniquely. In the isotropic limit, the potential energy is independent of θ and only $V_0(R)$ is retained in the Hamiltonian. Each isotropic state is then an eigenfunction of $\mathbf{j}^2$, $\mathbf{l}^2$, $\mathbf{J}^2$, and J_z, and may be labeled by $|jlJM\rangle$. The latter may be decomposed into a radial and an angular function:

$$|jlJM\rangle = \phi_{Jlj}(R)\mathcal{Y}^M_{Jlj}(\hat{r},\hat{R}) . \tag{3.2}$$

Due to the spherical harmonic properties of the angular function, the isotropic state has a definite parity of $(-1)^{j+l}$. (If the diatom is a homonuclear molecule, there is an additional symmetry of inversion of $\hat{r}$.) When the potential anisotropy is turned on, the state will be only an eigenfunction of $\mathbf{J}^2$ and J_z and of the same inversion parity $(-1)^{j+l}$. Nevertheless, the noncrossing rule ensures that the energy level for fixed J and M values and $(j+l)$ parity will not cross. Thus the isotropic function $|jlJM\rangle$ forms a convenient unperturbed basis for our present study.

According to the theory of dilatation transformation,[14] the energy (E_R) and the width (Γ) associated with a metastable predissociating state of an Ar...$H_2(j)$ complex may be determined by the solution of the complex eigenvalue of a non-Hermitian Hamiltonian $H_\alpha(R,\theta)$, obtained by applying the dilatation or complex-coordinate transformation[14] $R \to R\exp(i\alpha)$ to the real Hamiltonian $H(R,\theta)$, where α is usually taken to be a positive number. In the coupled-channel formalism,[9] the total wave function of the Hamiltonian $H_\alpha(R,\theta)$ for a given J and M is expanded in terms of the complete set of the isotropic state functions $|jlJM\rangle$ allowed by the symmetry. In order to *discretize* the vibrational continua, we further expand the radial function $\phi_{Jlj}(R)$ of $|jlJM\rangle$ in terms of an orthonormalized L^2 (square-integrable)-basis function $[\chi_n(R)]$:

$$\phi_{Jlj}(R) = \sum_{n=1}^{N_\gamma} a_n(\gamma)\chi_n(R) , \tag{3.3}$$

where γ specifies the channel quantum number, $\gamma = (jlJM)$, N_γ is the size of the truncated radial basis, and $\langle\chi_n|\chi_m\rangle = \delta_{nm}$. For convenience, let us define the basis function

$$|\gamma n\rangle \equiv \chi_n(R)\mathcal{Y}^M_{Jlj}(\hat{r},\hat{R}) \tag{3.4}$$

and arrange the order of the matrix elements of $H_\alpha(R,\theta)$ in such a way that n is allowed to vary from 1 to N_γ within each channel $\gamma = (jlJM)$. The matrix element in the $|\alpha n\rangle$ representation is

$$\langle\gamma' n'|H_\alpha(R,\theta)|\gamma n\rangle = \exp(-2i\alpha)\frac{\hbar^2}{2\mu}\langle\chi_{n'}|-\frac{d^2}{dR^2}+\frac{l(l+1)}{R^2}|\chi_n\rangle\delta_{ll'}\delta_{jj'}\delta_{JJ'}\delta_{MM'}$$
$$+B_{\rm rot}j(j+1)\hbar^2\delta_{ll'}\delta_{jj'}\delta_{nn'}\delta_{JJ'}\delta_{MM'}+\sum_{k=0,2}\langle\chi_{n'}|V_k(Re^{i\alpha})|\chi_n\rangle f_k(l'j',lj;J)\delta_{JJ'}\delta_{MM'} , \tag{3.5}$$

TABLE I. LJ(12, 6) potential parameters[d] characterizing the Ar–H_2 van der Waals complex studied in the present work.

Designation	V_0	ϵ (meV)	R_e (Å)	Aip1	Aip2	q_6	q_{12}	DSD
LJ(I)	Le Roy and van Kranendonk[a]	6.473[a]	3.557[a]	1.52[a]	0.095[a]	0.198[a]	0.301[a]	3.5[c]
LJ(II)	Le Roy and van Kranendonk[a]	6.473[a]	3.557[a]	1.35[c]	0.10[c]	0.154[c]	0.208[c]	1.1[c]
LJ(III)	Helbing *et al.*[b]	6.305[b]	3.34[b]	1.15[c]	0.10[c]	0.12[c]	0.14[c]	0.9[c]

[a]Reference 4(a).
[b]Reference 17.
[c]Reference 3(b).
[d]LJ(m, 6) potential has the following form: $V_0(R)=[\epsilon/(m-6)][6(R_e/R)^m - m(R_e/R)^6]$, $V_2(R)=[\epsilon/(m-6)] \times[6q_m(R_e/R)^m - mq_6(R_e/R)^6]$, where q_m, q_6 are related to the AIP (anisotropic intermolecular potential) parameters Aip1 and Aip2 in the following manner [Refs. 3(a) and 3(b)]: Aip1 $= q_m/q_6$ and Aip2 $= mq_6/6 - q_m$.

where f_k is the Percival–Seaton coefficient.[15] The resulting matrix of H_α is a symmetric complex matrix whose complex eigenvalues can be determined via the secular determinant

$$\mathrm{Det}\left|(H_\alpha)_{\gamma' n', \gamma n} - EI\right| = 0 \,. \tag{3.6}$$

The desired metastable states are then identified by the stationary points[10,14,20] of the α trajectories of complex eigenvalues.

IV. POTENTIAL SURFACES AND NUMERICAL METHODS

Zandee and Reuss[3(b)] have obtained anisotropic potentials $V_2(R)$ for the Ar–H_2 system based on their measurements of the orientationally dependent total collision cross sections and several isotropic potentials $V_0(R)$ taken from other independent investigations. They have considered two different types of potential forms, namely, Lennard-Jones (m, 6) potentials and Buckingham–Corner (BC) potentials. Several of the potentials obtained by Zandee and Reuss[3(b)] will be considered here.

Table I lists the three LJ(12, 6) potentials[3(b)] considered in the present study. The first LJ potential (both V_0 and V_2) is that obtained by Le Roy and van Kranendonk.[4(a)] In the second LJ potential, V_0 is that of Le Roy and van Kranendonk,[4(a)] whereas V_2 is determined by Zandee and Reuss.[3(b)] In the third LJ potential, V_0 is that obtained by Helbing *et al.*[17] and V_2 is again determined by Zandee and Reuss.[3(b)] From the DSD (dimensionless standard deviation)[3(b)] values, it is clear that potentials LJ (II) and LJ (III) provide better fits to the anisotropy experiments of Zandee and Reuss.[3(b)] The three LJ potentials are also depicted in Figs. 1(a)–1(c).

Table II lists the two BC(6, 8) potentials considered in the present study. In the first BC potential, V_0 is that obtained by Le Roy *et al.*[4(b)] It has been found[1] that this spherical potential provides excellent fits of the differential scattering cross sections of Rulis *et al.*[22] and the low-energy integral scattering cross sections of Toennies *et al.*[16] The V_2 part of the BC(I) potential is determined by Zandee and Reuss[3(b)] from their cross-section anisotropy experiments. In the second BC potential, both V_0 and V_2 are determined by Le Roy and Carley from the spectroscopic data.[4(d)] It is now generally believed[1] that the Buckingham–Corner potentials, BC(I) and BC(II), provide a more realistic description of the Ar $\cdots$ H_2 system than the LJ potentials describes in Table I. The two BC potentials are depicted in Fig. 1(d).

TABLE II. BC(6, 8) potential parameters[c] characterizing the Ar–H_2 van der Waals complex studied in the present work.

Designation	ϵ_0 (cm^{-1})	ϵ_2 (cm^{-1})	R_{e0} (Å)	R_{e2} (Å)	C_{60} (cm^{-1} Å^6)	C_{62} (cm^{-1} Å^6)	β (Å^{-1})	C_{82}/C_{80}
BC(I)[a]	50.84	5.034	3.5735	3.72	136 400	14 590	3.692	0.170
BC(II)[b]	50.87	5.72	3.5727	3.743	134 500	13 500	3.610	0.248

[a]Reference 3(b).
[b]Reference 4(d).
[c]This potential has the following form ($n=0, 2$):

$$V_n(R) = A_n \exp(-\beta R) - (C_{6_n} R^{-6} + C_{8_n} R^{-8}) D(R) \,,$$

$$D(R) = \exp[-4(R_{en}/R - 1)^3] \,, \quad R \leqq R_{en} \,,$$

$$= 1 \,, \quad R \geqq R_{en} \,,$$

and

$$A_n = (8\epsilon_n - 2C_{6_n} R_{en}^{-6}) \exp(\beta R_{en})/(\beta R_{en} - 8) \,,$$

$$C_{8_n} = [R_{en}^8/(\beta R_{en} - 8)] \cdot [(6 - \beta R_{en}) C_{6_n} R_{en}^{-6} + \epsilon_n \beta R_{en}] \,.$$

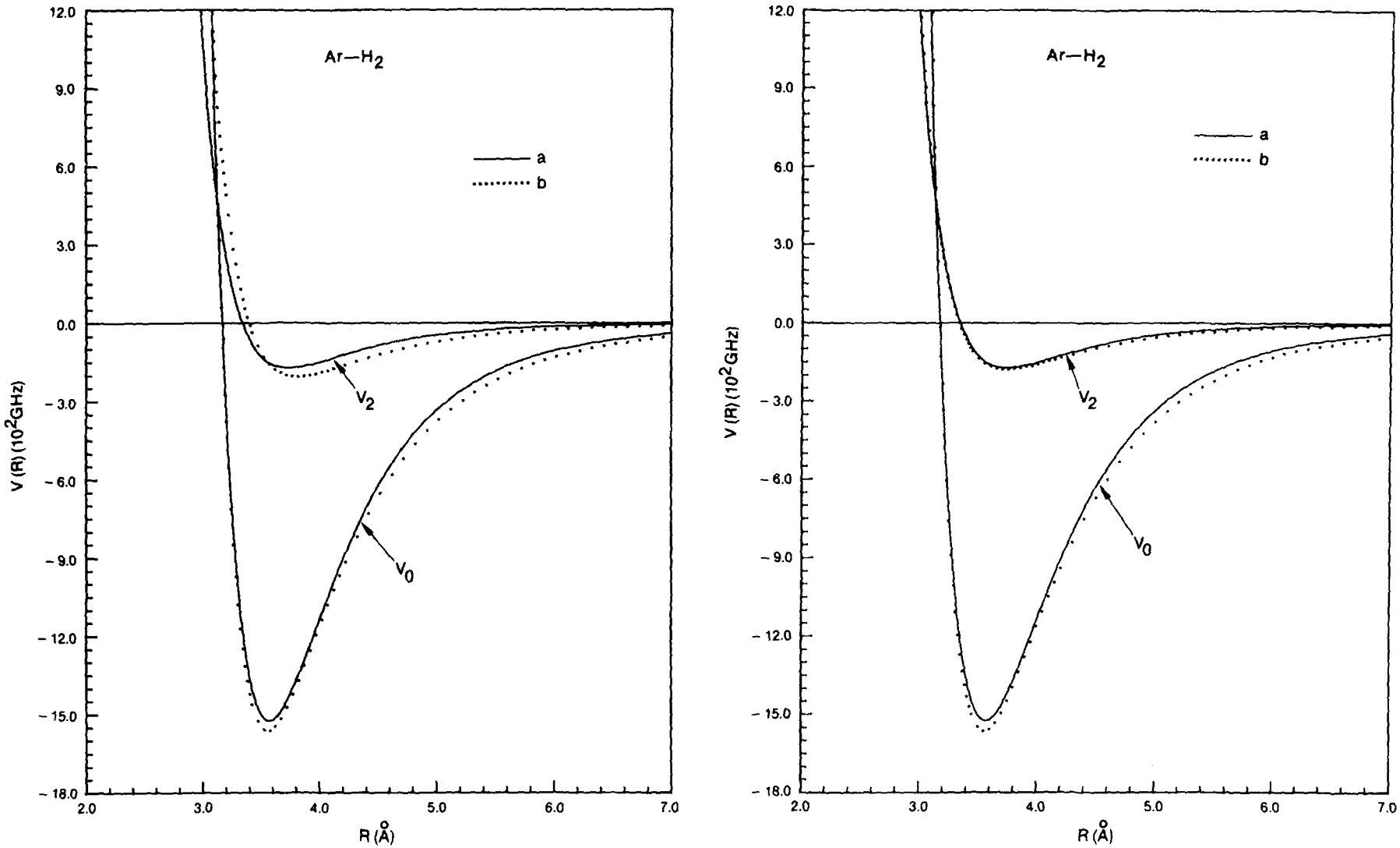

FIG. 1. Potential surfaces $V_0(R)$ and $V_2(R)$ of the Lennard-Jones (LJ), Buckingham–Corner (BC), and Tang–Toennies (TT) potentials listed in Tables I–III. The BC(II) surfaces (indicated by solid curves or a are used here as references for comparison purpose. Other surfaces are indicated by dotted curves of b). (a) LJ(I) vs BC(II); (b) LJ(II) vs BC(II); (c) LJ(III) vs BC(II); (d) BC(I) vs BC(II); (e) TT vs BC(II).

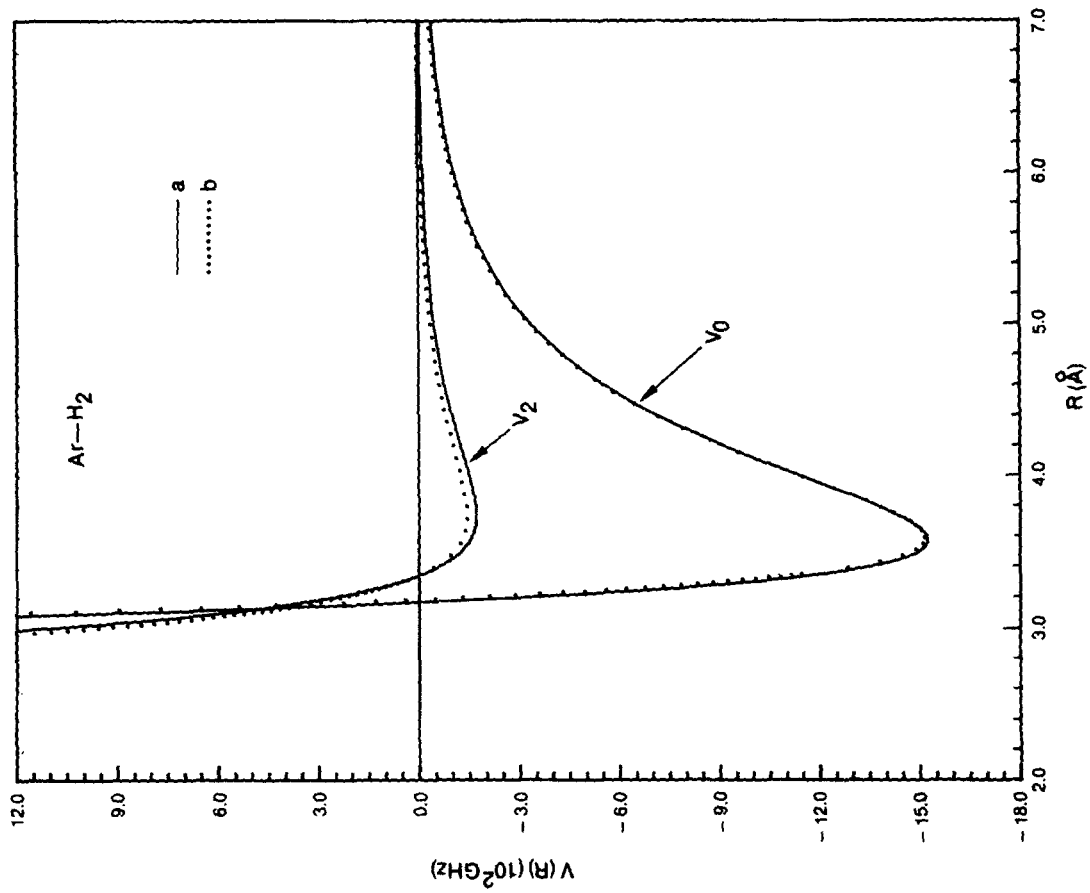

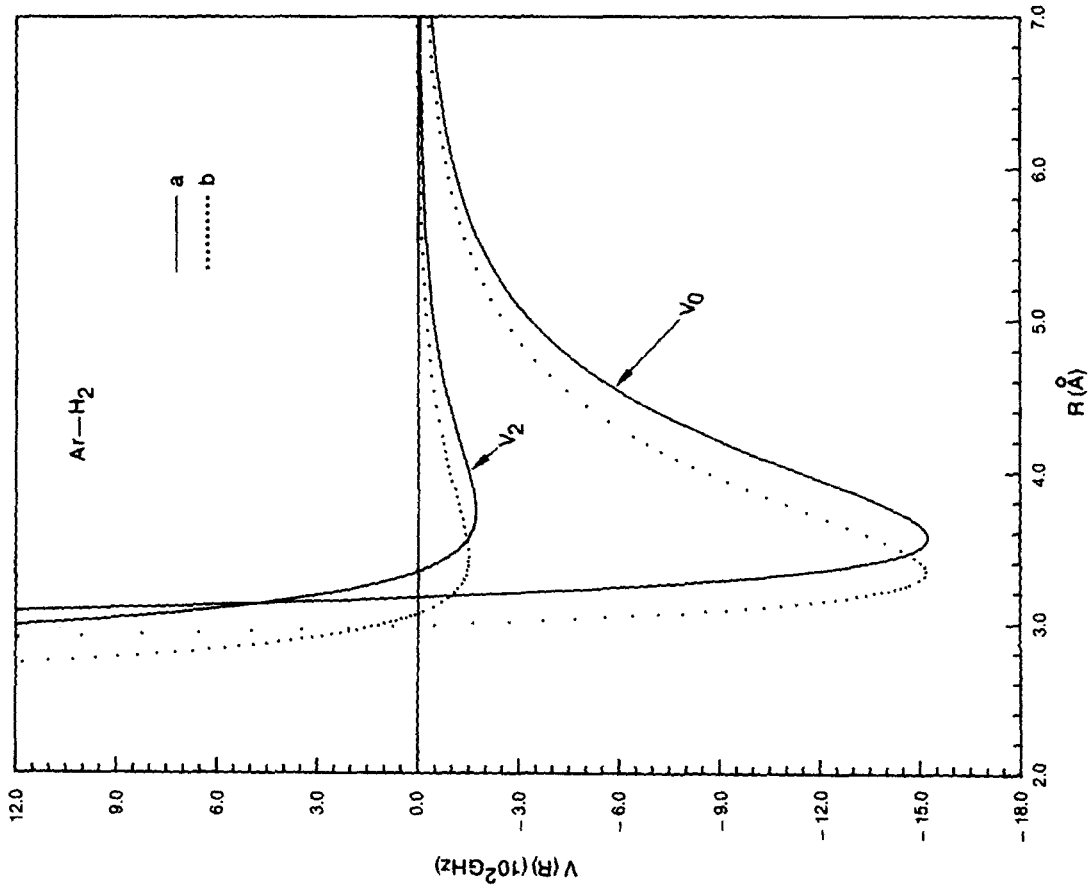

FIG. 1. (*Continued*)

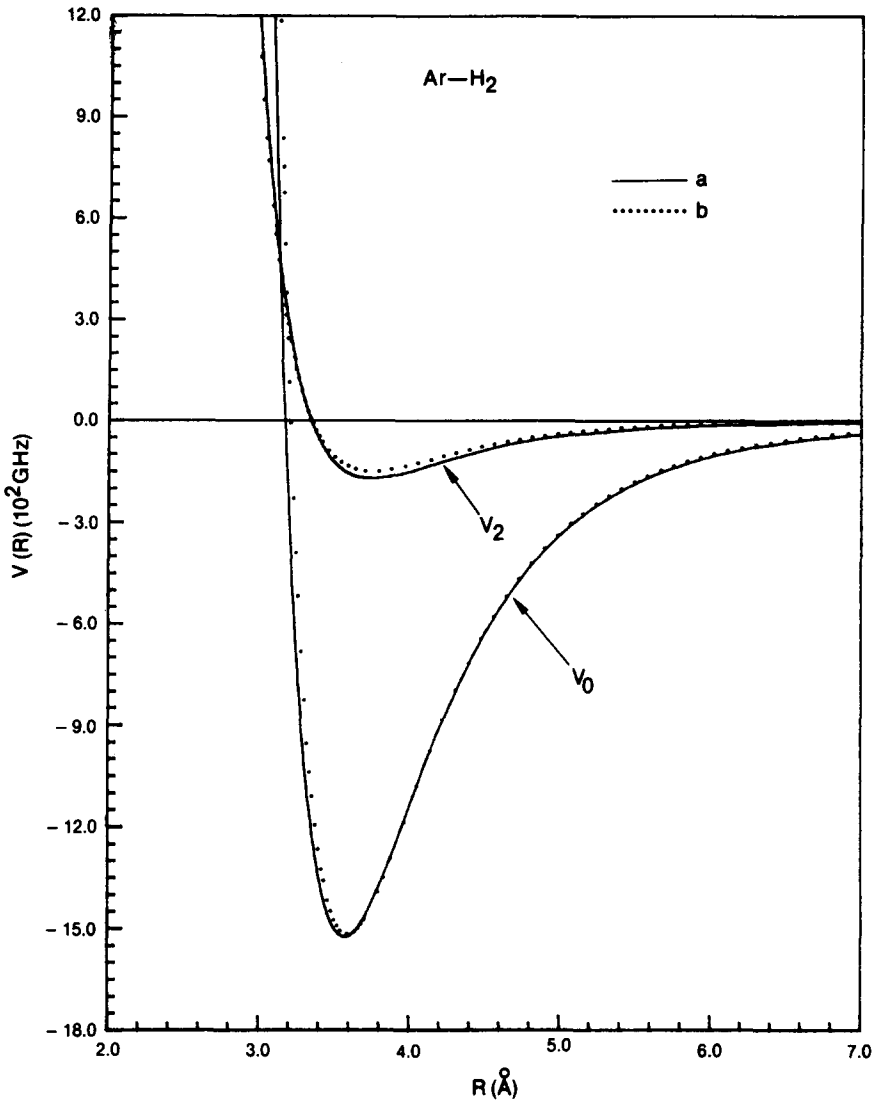

FIG. 1. (*Continued*)

The last potential we consider here is the semi-empirical potential proposed recently by Tang and Toennies.[12(c)] They found that the cross section anisotropy factors derived from this potential are in very good agreement with the experimental data measured by Zandee and Reuss.[3(b)] The potential of Tang and Toennies (TT) consists of repulsive potential, determined by application of Gilbert–Smith combining rules,[12(c)] and of attractive potential with dispersion terms estimated using precise combining rules.[12(b)] The expression for the TT potential is ($n=0,2$)

$$V_n = V_{\mathrm{SCF}n} - V_{\mathrm{disp}n} + V_{\mathrm{corr}n}\,, \tag{4.1}$$

where V_{SCF} is the SCF repulsive energy, V_{disp} is the dispersion energy, and V_{corr} is the coupling correction. The individual terms in Eq. (4.1) are modeled by the analytic forms[12(c),21] described in the Appendix. The molecular parameters of the TT potential for the $Ar\cdots H_2$ system are listed in Table III, and the potential curves are shown in Fig. 1(e).

For all the six potentials discussed above, we consider the excitation of Ar and H_2 such that the collision energy $E < E_{\mathrm{th}}(=6B_{\mathrm{rot}})$, the threshold for the first allowed rotational transition ($j=0\rightarrow 2$). In particular, we focus on the metastable state which correlates with the isotropic channel $|j=2, l=2, J=0, M=0\rangle$. Because of the symmetry of H_2, only the following angular basis need be considered: ($j=0$, $l=0$), ($j=2$, $l=2$), ($j=4$,

TABLE III. TT potential parameters[a,b] for the Ar–H_2 van der Waals complex.

$A_{\parallel}$	46.4
$A_{\perp}$	45.0
$b_{\parallel}$	1.752
$b_{\perp}$	1.804
M(Ar)	0.0318
$M(H_2)_{\parallel}$	0.0903
$M(H_2)_{\perp}$	0.0956
Γ_6	0.102
Γ_8	0.248
Γ_{10}	0.30
C_6	28.4
C_8	576.0
C_{10}	14600

[a]In atomic units.
[b]Reference 12(c).

$\langle j=l=0,n \mid H \mid j'=l'=0,n' \rangle$	$\langle j=l=0,n \mid V_2P_2 \mid j'=l'=2,n' \rangle$	0
$\langle j=l=2,n \mid V_2P_2 \mid j'=l'=0,n' \rangle$	$\langle j=l=2,n \mid H \mid j'=l'=2,n' \rangle$	$\langle j=l=2,n \mid V_2P_2 \mid j'=l'=4,n' \rangle$
0	$\langle j=l=4,n \mid V_2P_2 \mid j'=l'=2,n' \rangle$	$\langle j=l=4,n \mid H \mid j'=l'=4,n' \rangle$

$(n,n'=1,2,\ldots\ldots,N)$

FIG. 2. Matrix structure of the predissociation Hamiltonian H in the $|\gamma n\rangle$ representation. Here $\gamma=(jl, J=M=0)$ specifies the channel quantum numbers, n is the index number for the harmonic oscillator radial basis, $n=1, 2, \ldots, N$, and V_2P_2 is the anisotropic potential.

$l=4),\ldots$, etc. For the $Ar-H_2$ system, we found that the resonance energy and width (lifetime) of the metastable state can be determined satisfactorily by including the only open channel ($j=0, l=0, J=0$, $M=0$) and one closed channel ($j=2$, $l=2$, $J=0$, $M=0$). Very high precision can be achieved by including one additional closed channel ($j=4$, $l=4$, $J=0$, $M=0$) in the basis set.

The matrix structure in the $|\gamma n\rangle$ representation is of three by three block form (for the three-channel case), as depicted in Fig. 2. Within each diagonal block specified by the channel quantum number $\gamma=(jlJM)$, we use the orthonormal harmonic oscillator L^2 basis

$$\chi_n(R)=\left(\frac{\beta}{\pi^{1/2}2^n n!}\right)^{1/2} H_n(\beta x)\exp(-1/2\beta^2x^2)\ , \qquad n=1,2,\ldots,N_\gamma \tag{4.2}$$

to expand the radial wave function $\phi_{Jlj}(r)$ defined in Eq. (3.2). It is well known[9,18] that the harmonic oscillator basis provides a compact analytic representation for the complete set of bound and continuum states of an anharmonic oscillator in the inner radial region. In Eq. (4.2), H_n is a Hermite polynomial, $x=R-R_0$, and β is an adjustable nonlinear parameter.

As far as the complex coordinate transformation is concerned, the LJ $(m,6)$ potentials have the advantage in that they are homogeneous in the radial distance R. Thus, the potential matrix elements need be computed only once. This is not the case for the inhomogeneous piecewise BC and TT potentials, where the potential matrix elements have to be recomputed for each new rotational angle α. The BC and especially the TT potentials, however, pose new challenges to the utility of the complex coordinate transformation. It has not been shown previously that the dilatation analyticity can be preserved in the whole range of R for piecewise potentials which have different analytic forms in different radial ranges. Indeed, as will be shown below, the direct computation of the complex rotated potential matrix elements $\langle\chi_{n'}|V_h(Re^{i\alpha})|\chi_n\rangle$ using the procedure suggested in Ref. 9 and discussed immediately below works best only for the LJ$(m,6)$ type potentials. Appropriate new numerical techniques have had to be introduced to deal with the BC and TT potentials.

In the case of LJ$(m,6)$ type homogeneous potentials, the best procedure to compute the potential matrix elements is to adopt the orthonormal harmonic oscillator basis described in Eq. (4.2) and to use the quadrature procedure devised by Harris *et al.*[9,28] Thus,

$$\langle\chi_{n'}|R^{-m}|\chi_n\rangle \simeq \sum_{s=1}^{N} T_{n's}T_{ns}\left[\frac{\xi(s)}{\beta}+R_0\right]^{-m}\ . \tag{4.3}$$

Here $T=(T_{pq})$ is the orthogonal matrix which diagonalizes the matrix (ξ_{pq}) of the operator $\xi=\beta x=\beta(R-R_0)$ in the harmonic oscillator basis of truncated size N, and $\xi(s)$ is the corresponding sth eigenvalue.[9] Once the potential matrix elements have been computed, the symmetric complex matrix as depicted in Fig. 2 can be set up and the complex eigenvalue of the metastable state correlates with the isotropic channel $|j=l=2$, $J=M=0\rangle$ can be found.[19] To facilitate the location of the optimum α trajectory, the parameters R_0 and β can be adjusted in such a way that the *spurious widths*[23] associated with the unperturbed diagonal complex eigenvalues (i.e., the imaginary parts of the eigenvalues of the diagonal block $\langle j=l=2, n|H_\alpha|j'=l'=2,n'\rangle$ that are correlated with the predissociation resonances) be kept as small as possible. As a practical guide for multichannel problems, it is important that these (unperturbed) spurious widths be smaller in magnitude than the genuine (perturbed) predissociation widths of physical interest. In the case of LJ$(m,6)$ potentials, the spurious widths decrease rapidly with increasing N, and one can easily find a wide range of R_0 and β parameters such that the spurious widths are many orders of magnitude smaller than the physical widths.

Typical examples of the α trajectories are shown in Figs. 3–5 for LJ(I)–LJ(III). It is seen that the resonance positions are clearly identified by the sharp stationary points [where $d(E_R+i\Gamma/2)/d\alpha\approx 0$] in the α trajectories. Table IV shows a typical example of the convergence of the resonance positions with respect to the basis size N_γ [potential LJ(III)]. We note that E_R (=real

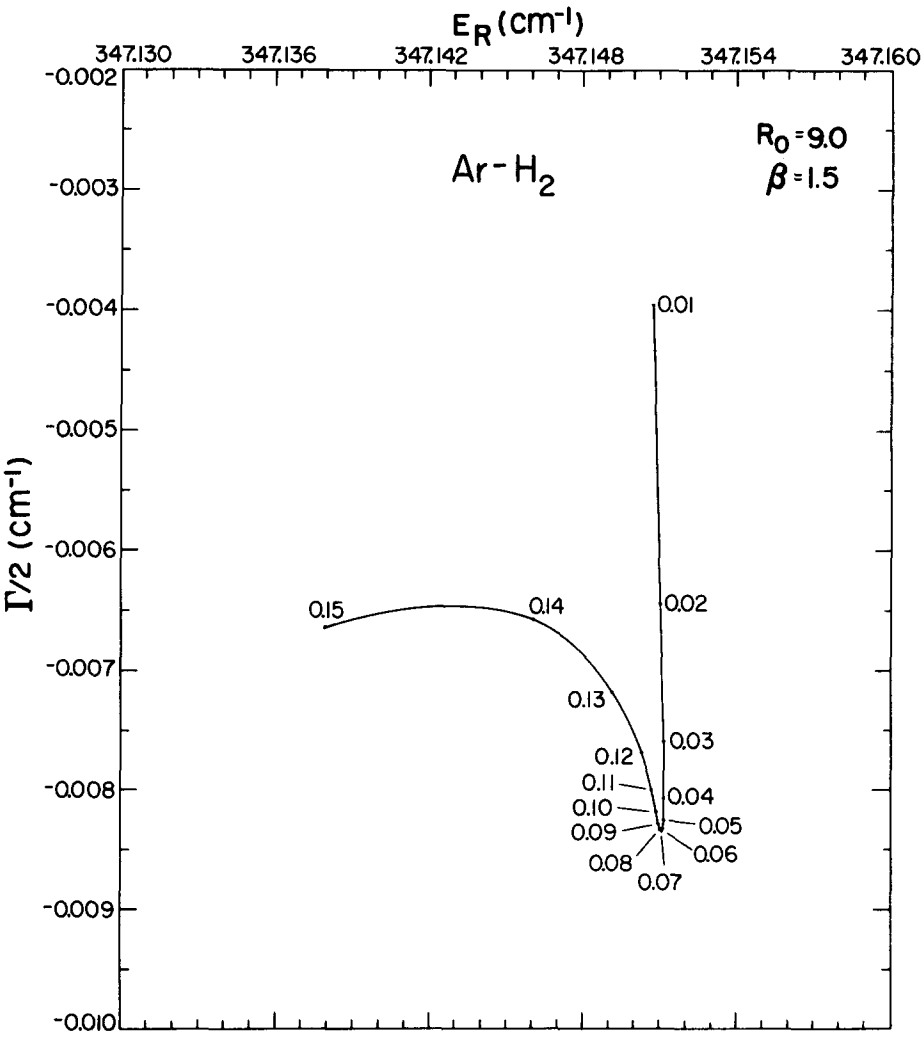

FIG. 3. A typical α trajectory for the complex eigenvalue associated with the rotational predissociation of the metastable level ($j = l = 2$, $J = M = 0$) of the Ar ··· H_2 van der Waals molecule [with potential LJ(III)]. The numbers on the dots shown in the figure indicate the rotational angles (in radians) used. These are three-channel-block calculations with $N = 50$ for each block.

part of the complex eigenvalue) converges to within 10^{-3} cm^{-1} with $N_\gamma > 30$, and to within 10^{-4} cm^{-1} with $N_\gamma > 40$. The convergence of the half-width ($\Gamma/2$ or imaginary part of the complex eigenvalue) is somewhat slower: $N_\gamma = 35$ is needed to converge $\Gamma/2$ to within 10^{-3} cm^{-1} and $N_\gamma = 45$ to within 10^{-4} cm^{-1}.

We next consider the predissociation calculations of the BC(6, 8) type potentials. The complex potential matrix elements can be evaluated using a formula similar to Eq. (4.3), namely,

$$\langle \chi_{n'} | V(Re^{i\alpha}) | \chi_n \rangle = \sum_{s=1}^{N} T_{n's} T_{ns} [V(R(s)e^{i\alpha})] , \qquad (4.4)$$

where $R(s) = \xi(s)/\beta + R_0$ and $V[R(s)e^{i\alpha}]$ can be computed analytically for BC potentials. Using matrix elements generated by this R-rotation method [Eq. (4.4)], we found that the unperturbed spurious widths are substantially larger than the corresponding ones in LJ potentials (though they are still somewhat smaller than the physical widths). Furthermore, these BC spurious widths do not decrease (or even not decrease at all) with increasing N as rapidly as those of LJ potentials.[31] This poses some difficulty for the R-rotation method to achieve high accurate results for the BC potentials.

Recently we found, however, an alternative procedure[24] which is capable of decreasing the spurious widths by orders of magnitude and rapidly improves the convergence of lifetime calculations. In this procedure, we rewrite the potential $V(R)$ as $V(X + R_0)$, where V is either V_0 or V_2, $X = R - R_0$, and R_0 is an adjustable parameter which is usually taken to be somewhat greater than the equilibrium distance of V_0. The appropriate

TABLE IV. Convergence study of the position of the resonance state ($l = j = 2$, $J = M = 0$) of the Ar ··· H_2 van der Waals molecule [potential LJ(III)] with respect to basis size N_γ. Shown here are calculations with two channel blocks (with the same basis size N_γ), and $R_0 = 9.0 a_0$, $\beta = 1.5 a_0^{-1}$ (a_0 = Bohr radius), and rotational angle $\alpha = 0.07$ rad.

N_γ	E_R (cm^{-1})	$\Gamma/2$ (cm^{-1})
20	347.2774	0.0327
30	347.1553	0.0105
35	347.1541	0.0090
40	347.1539	0.0087
45	347.1539	0.0085
50	347.1539	0.0083
60	347.1539	0.0083

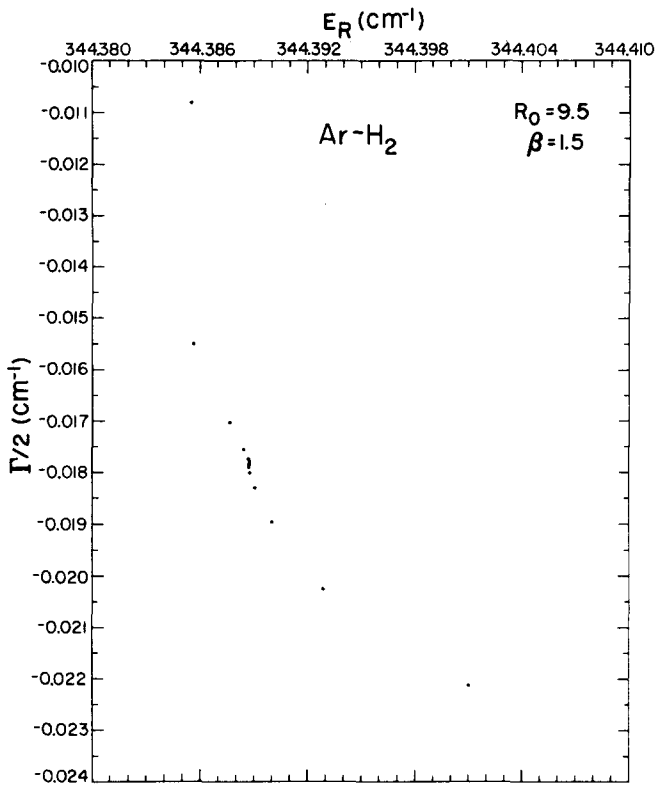

FIG. 4. A typical two-channel block (with $N=50$ for each block) α trajectory for the Ar $\cdots$ H_2 metastable state ($j=l=2$, $J=M=0$) with potential LJ(II).

complex rotation in the X coordinate[29] is now

$$V(X+R_0) \to V(Xe^{i\alpha}+R_0)\ , \tag{4.5}$$

and the complex potential matrix elements can be computed by the formula

$$\langle \chi_{n'} | V(Xe^{i\alpha}+R_0) | \chi_n \rangle \simeq \sum_{s=1}^{N} T_{n's} T_{ns} [V(X_s e^{i\alpha}+R_0)]\ , \tag{4.6}$$

where $X_s=\xi(s)/\beta$ and $V(X_s e^{i\alpha}+R_0)$ can be calculated completely analytically for BC potentials. We note that in this X-rotation method, the basis function $\chi_n(X)$ has the same form as Eq. (4.2) except with only one disposable parameter β. The other parameter, R_0, has now been absorbed into the potential function itself. Formally speaking, the potential $V(X+R_0)$ with R_0 a constant is just an alternative representation of the original potential $V(R)$. Thus the X- and R-rotation methods should give rise to the same physical results. Indeed, we have tested this idea in several examples, including tunneling in the anharmonic oscillator,[25] orbiting resonances of rare gas-H_2 van der Waals systems,[26] and multichannel predissociation of Ar $\cdots$ N_2 van der Waals molecules.[24] Clearly, the X-rotation method has no practical advantage for homogeneous type potentials such as LJ's. However, for simple inhomogeneous type such as BC potentials, it could be very fruitful.

Using the X-rotation procedure and the formula (4.6), we have carried out the predissociation calculations for the two BC(6,8) potentials listed in Table II. The unperturbed spurious widths (typically 10^{-10} a.u.) are now comparable in magnitude to those of LJ's and decrease rapidly with increasing N. Typical examples of the α trajectories are shown in Figs. 6 and 7 for BC(I) and BC(II), respectively. Examination of the convergence of the resonance positions with respect to the basis size N_γ indicates that the quality of the BC results using the X-rotation method is about as good as that of the LJ results using the R-rotation method. The reason why the X-rotation method works better for BC potentials is not completely clear. However, one tentative explanation is that for physical problems involving harmonic oscillator type potential wells, X is perhaps the more and natural coordinate for describing the vibrational stretching of the van der Waals bond.

The last potential we consider is the highly inhomogeneous Tang-Toennies (TT) potential. As shown earlier, the TT potential consists of many radial intervals each of which has a different analytic potential functional form. There exists no previous demonstration that the complex coordinate transformation can be applied successfully to a complicated piecewise analytical potential such as TT's. Direct computation of the potential matrix elements using the R-rotation method [Eq. (4.4)] gives unperturbed spurious widths hopelessly too large (typically about one to two orders of magnitude larger than the physical widths). The X-rotation method [Eq. (4.6)] improves the results substantially but is still not fine enough to give high accurate results as quoted for LJ and BC potentials. This indicates some numerical

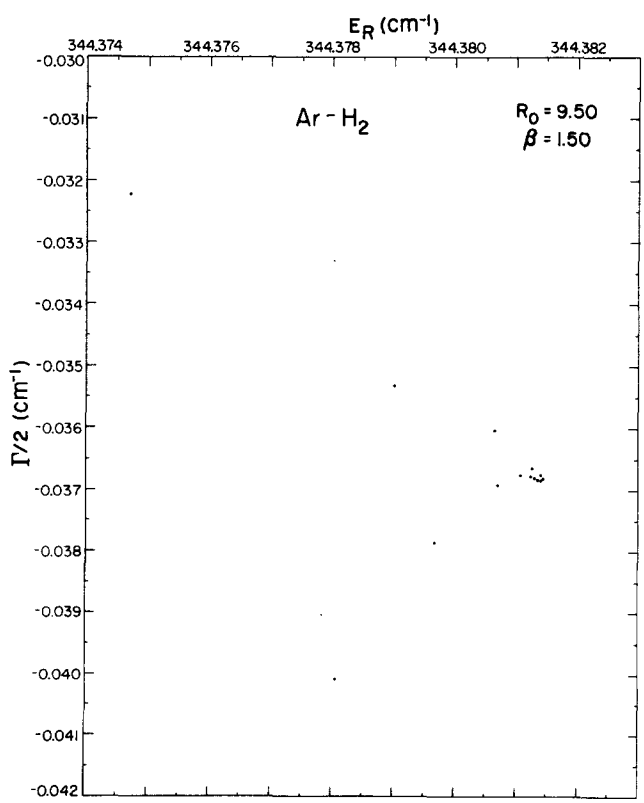

FIG. 5. A typical two-channel block (with $N=50$ for each block) α trajectory for the Ar $\cdots$ H_2 metastable state ($j=l=2$, $J=M=0$) with potential LJ(I).

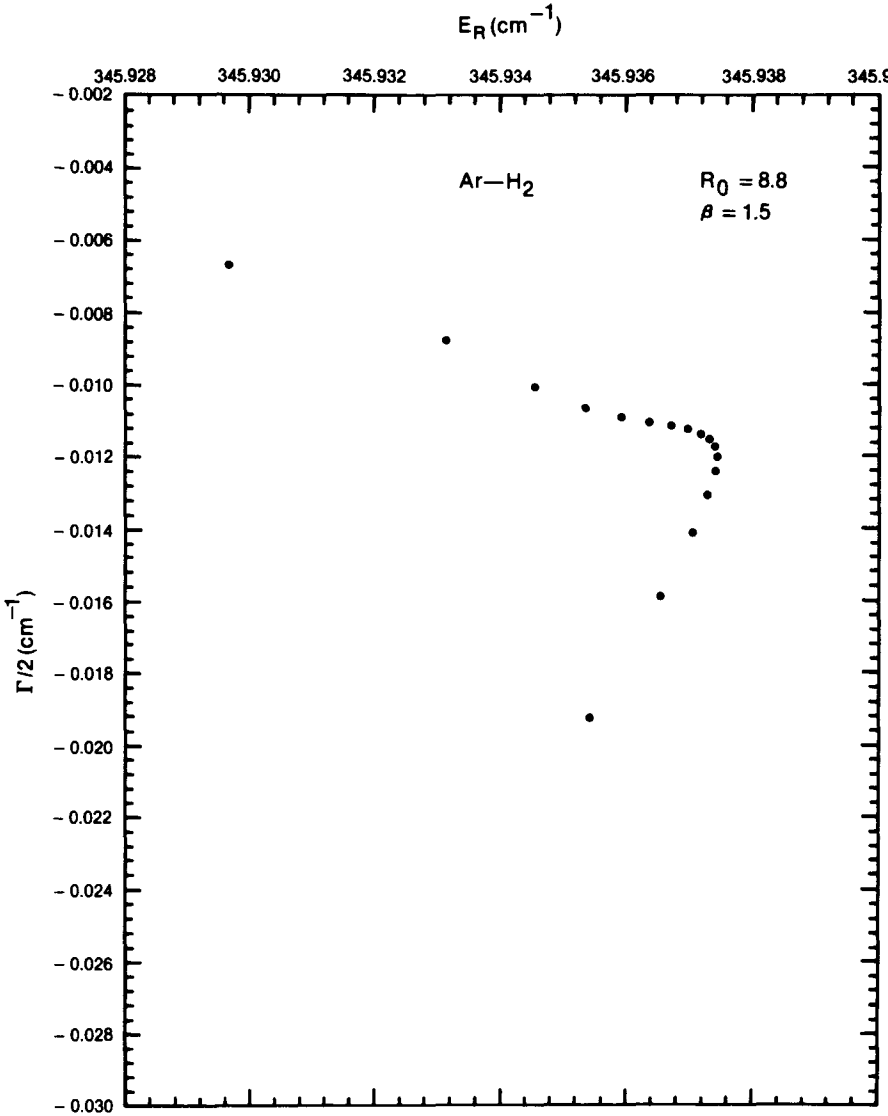

FIG. 6. A typical two-channel block (with $N = 50$ for each block) α trajectory for the Ar $\cdots$ H_2 metastable state ($j = l = 2, J = M = 0$) with potential BC(I).

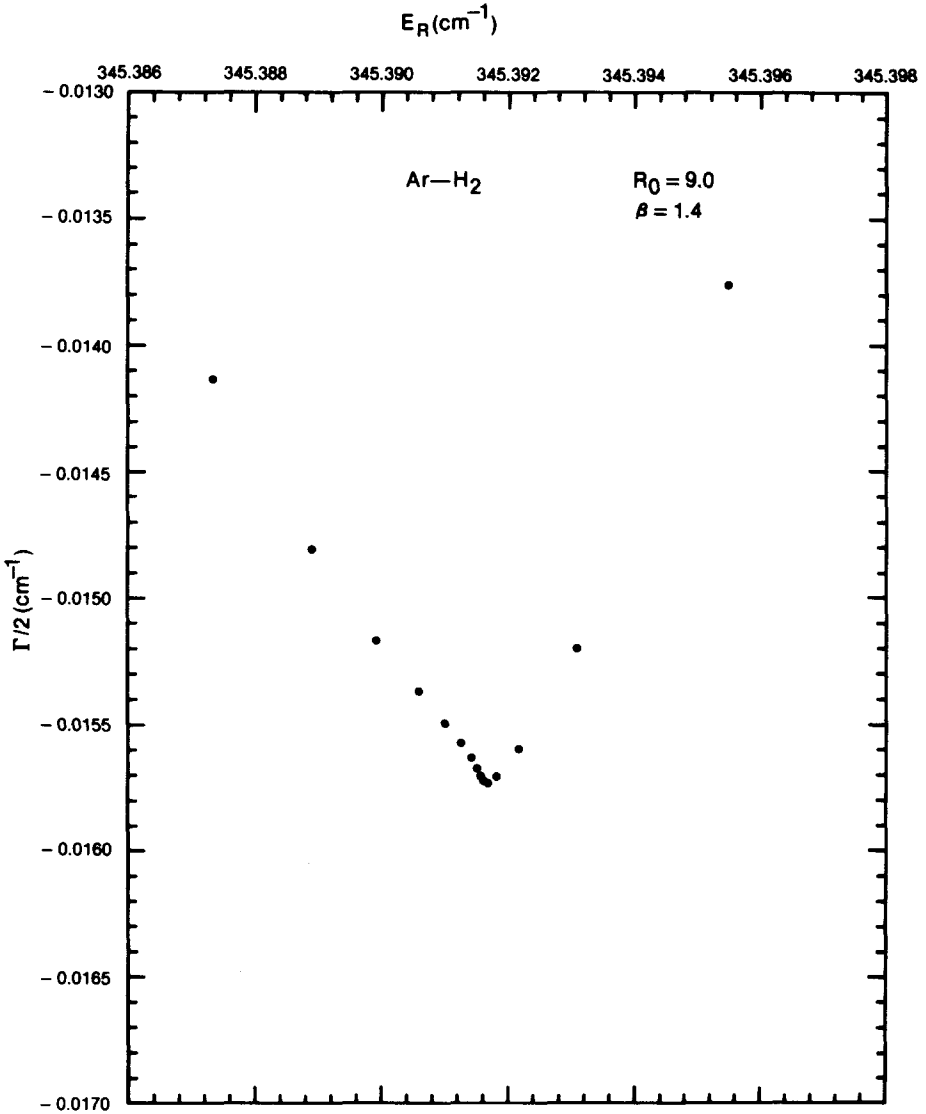

FIG. 7. A typical two-channel block (with $N = 50$ for each block) α trajectory for the Ar $\cdots$ H_2 metastable state ($j = l = 2, J = M = 0$) with potential BC(II).

instabilities associated with the direct computation of the potential matrix elements.

The best procedure to deal with a complicated piecewise analytic potential is perhaps *not* to compute the matrix elements of the complex rotated potential $V(Re^{i\alpha})$ or $V(Xe^{i\alpha}+R_0)$ directly but to use an indirect way, as described below. Recently we have developed a computational scheme[24] for dealing with the complex coordinate transformation of *numerical* potentials (i.e., potentials are given in tabulated numerical forms rather than in specified analytic forms). This method has been applied successfully to the multichannel predissociation of the Ar $\cdots$ N_2 system[24] involving four closed and four open channels. A suitable extension of this new procedure, described below, provides stable algorithms for solving the TT potential problem. This method, which takes advantage of several well established transformation theories and quadrature algorithms, consists of the following three steps.

Step (i). The identity

$$\langle\chi_i(y)|\,V(ye^{i\alpha})\,|\chi_j(y)\rangle = e^{-i\alpha}\langle\chi_i(ye^{-i\alpha})|\,V(y)\,|\chi_j(ye^{-i\alpha})\rangle \tag{4.7}$$

is used to transform the complex rotated potential $V(ye^{i\alpha})$ back to the real potential $V(y)$. In Eq. (4.7), the coordinate y can be either R or X.

Step (ii). The inner projection technique[24,27] is adopted such that

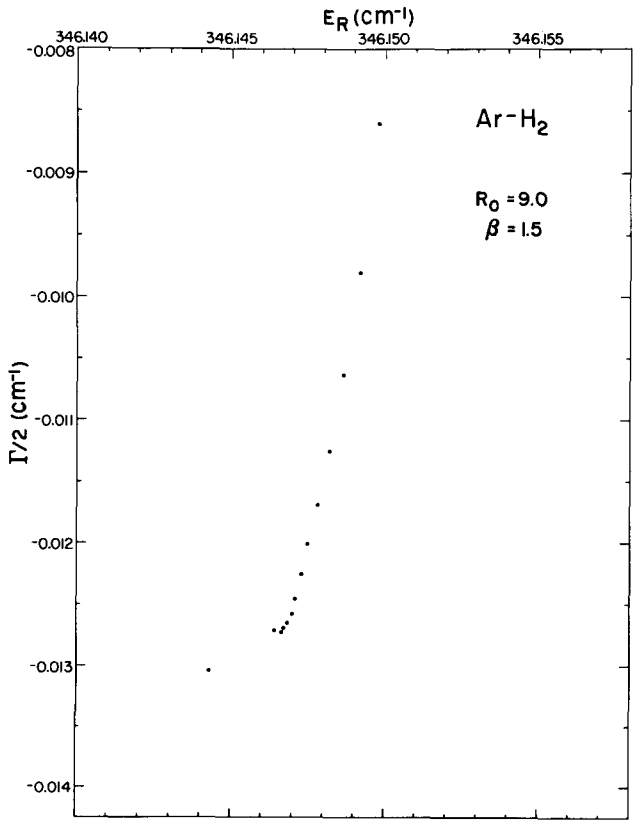

FIG. 8. A typical two-channel block (with $N=40$, $M=60$ for each block) α trajectory for the Ar $\cdots$ H_2 metastable state ($j=l=2$, $J=M=0$) with potential TT.

TABLE V. Summary of the converged resonance positions of the metastable Ar $\cdots$ H_2 complex (with $l=j=2$, $J=M=0$) obtained in the present study. All channel blocks have the same basis size $N_\gamma=50$.

Potential designation	No. of channel blocks	E_R (cm^{-1})	$\Gamma/2$ (cm^{-1})
LJ(I)	2	344.3814	0.0369
LJ(I)	3	344.3726	0.0371
LJ(II)	2	344.3887	0.0179
LJ(II)	3	344.3837	0.0179
LJ(III)	2	347.1539	0.0083
LJ(III)	3	347.1510	0.0083
BC(I)	2	345.9374	0.0118
BC(I)	3	345.9341	0.0118
BC(II)	2	345.3916	0.0158
BC(II)	3	345.3871	0.0158
TT	2	346.1467	0.0127
TT	3	346.1433	0.0127

$$\langle\chi_i(ye^{-i\alpha})|\,V(y)\,|\chi_j(ye^{-i\alpha})\rangle = \sum_{\alpha\beta}^{M}\langle\chi_i(ye^{-i\alpha})|\,\phi_\alpha(y)\rangle \times\langle\phi_\alpha(y)|\,V(y)\,|\phi_\beta(y)\rangle\cdot\langle\phi_\beta(y)|\,\chi_j(ye^{-i\alpha})\rangle\,, \tag{4.8}$$

where $\{\phi_\alpha(y)\}$ are real, L^2-orthonormal basis functions, such as those of Eq. (4.2), and M is the number of inner basis functions used. The simplifying feature here is that the evaluation of the complex rotated-potential matrix is now replaced by the much simpler calculations of the *complex overlap matrix* as well as the matrix elements of *real* potentials. The complex overlap matrix elements $\langle\chi_i(ye^{-i\alpha})|\,\phi_\alpha(y)\rangle$ can be written in closed analytic forms and evaluated exactly for the harmonic oscillator basis.[30] Thus the uncertainty associated with the direct computation of the matrix elements of complex rotated potentials can be removed.

Step (iii). The matrix elements of the real potential (in numerical or sophisticated analytic forms such as TT's), $\langle\phi_\alpha(y)|\,V(y)\,|\phi_\beta(y)\rangle$ can also be evaluated accurately using either formula (4.4) or (4.6) with the rotational angle α setting equal to zero.

With this three-step procedure, we have performed the predissociation calculations for the TT potential listed in Table III and shown in Fig. 1(e). The unperturbed spurious widths (typically 10^{-10} a.u.) are now comparable in magnitude to those of LJ's and BC's and decrease uniformly with increasing N. A sufficient number of inner basis functions, i.e., M, must be included to ensure the complete convergence of potential matrix elements. In the case of the TT potential, we found that the choice $M \geq N+20$ is adequate for high precision calculations. Shown in Fig. 8 is a typical example of the α trajectory for the TT potential for the case $N=40$ and $M=60$. The desired resonance position is clearly indicated by the sharp kink point. We thus see that this alternative procedure is capable of providing stable numerical algorithms for the accurate computation of the resonance energies for sophisticated analytic potentials.

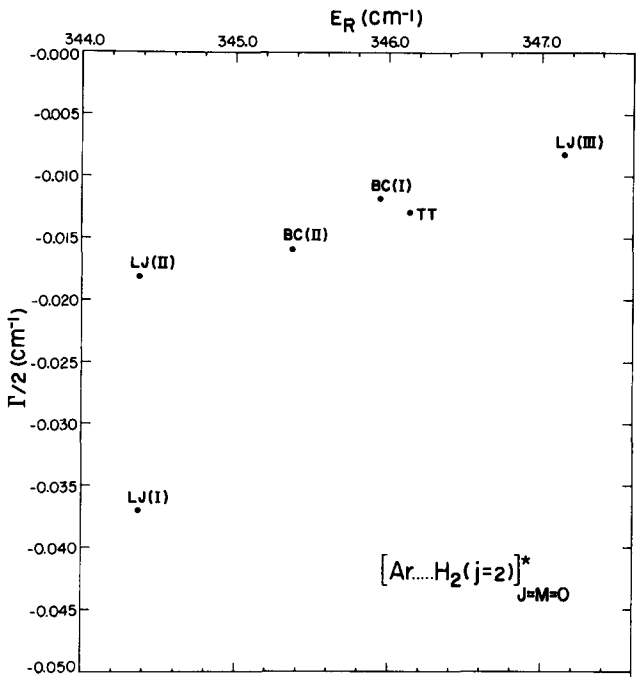

FIG. 9. Summary of the predicted resonance positions for the six potential surfaces considered: LJ(I)–LJ(III), BC(I), BC(II), and TT.

V. RESULTS AND DISCUSSION

Finally, we summarize the converged results of the resonance positions obtained in this study in Table V. We note that the two-channel block [one open channel ($j=l=0$) and one closed channel ($j=l=2$)] calculations for the Ar···H_2 system are sufficient to achieve the accuracy of the resonance energies (for a given potential surface) to within 0.01 cm^{-1}. The inclusion of an additional ($j=l=4$) closed channel block (i.e., the three-channel-block case) mainly affects the E_R values and is appreciable only when the anisotropy is strong[32] [such as LJ(I)]. Calculations with more than three-channel blocks for the Ar···H_2 system appear unnecessary.

The three-channel-block results with $N_\gamma=50$, listed in Table V, represent the best data obtained in this study. We conclude that for a given potential surface the complex-coordinate coupled-channel formalism[9] together with appropriate numerical computational schemes is capable of providing a reliable determination of the resonance energies as well as the linewidths (lifetimes) of the rotationally predissociating states of the Ar···H_2 system to within 10^{-3} cm^{-1}. Furthermore, the predicted linewidths (lifetimes) and energies are sensitive to the potential surfaces used. Shown in Fig.

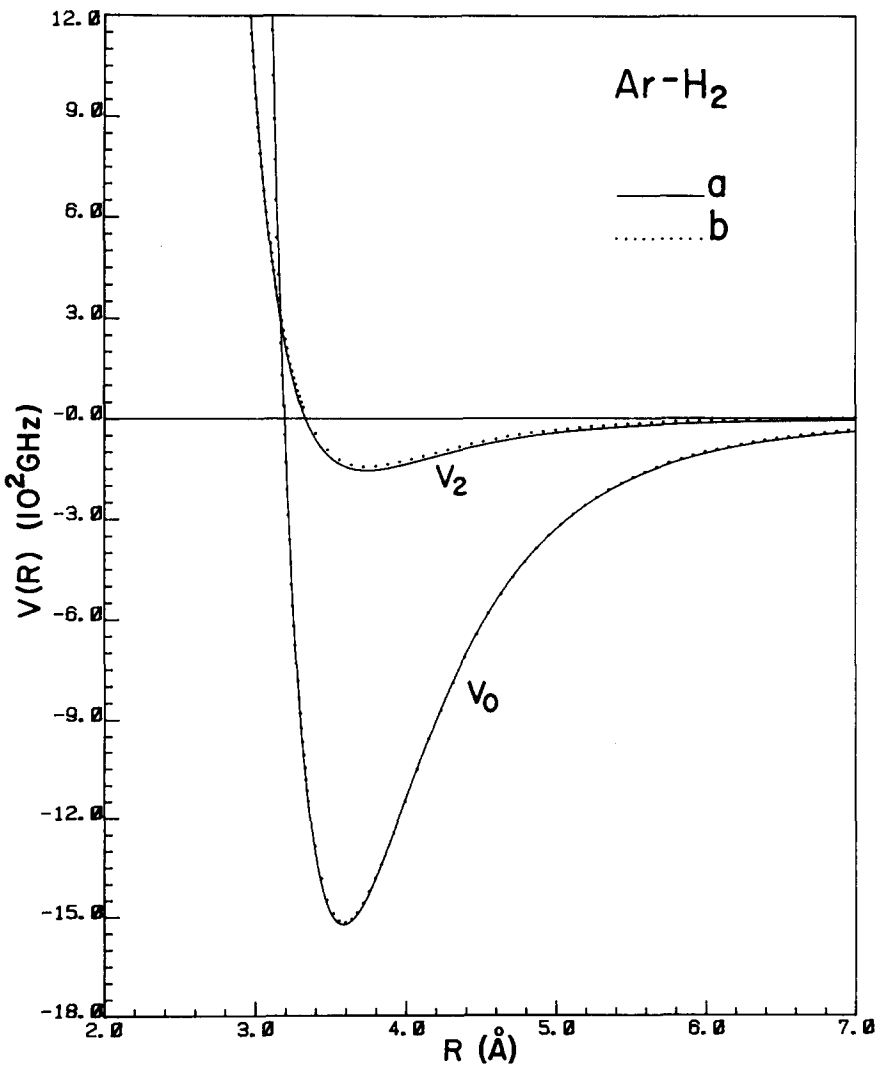

FIG. 10. Comparison of the potential surfaces of BC(I) [dotted curves or (b)] and TT [solid curves or (a)].

9 is the comparison of the predicted resonance positions (three-channel-block converged results) for the potential surfaces considered in this study.[33] We note that the linewidths predicted for the (less accurate) LJ potentials vary by a factor as large as 4. However, the agreement among more recent potentials, namely, BC(I), BC(II), and TT, is much closer: the resonance energies (E_R) agree to within 1 cm^{-1} and the linewidths (Γ) to within 30%. In particular, the agreement between BC(I) and TT can be considered rather satisfactory.

Finally, it is instructive to compare the predicted results with the potential curves depicted in Figs. 1(a)–1(e), where the BC(II) curves V_0 and V_2 are used as references for comparison purposes. Close examination of the curves reveals that the results given in Table V and Fig. 9 are in harmony with the dynamics of rotational predissociation, namely, stronger anisotropic potentials favor larger linewidths and vice versa. It is also interesting to see that the BC(I) and TT potential surfaces do show the closest agreement (Fig. 10) of all, in accordance with the predicted results. We note, however, that Waaijer[21] has recently completed a very accurate determination of the hyperfine spectroscopy of Ar···H_2 van der Waals molecules. His results indicate that, although the BC(II) and TT potentials are among the most accurate ones determined to date, they are still not completely consistent with the hyperfine structure data, suggesting that further refinement of the anisotropic potentials may be possible.

ACKNOWLEDGMENTS

This research was supported in part by the United States Department of Energy under contract No. DE-AC02-80ER10748, by the Research Corporation, and by the Alfred P. Sloan Foundation. Acknowledgment is also made to the Donors of the Petroleum Research Fund, administered by the American Chemical Society, for partial support of this work.

APPENDIX

The potential of Tang and Toennies (TT) consists of a repulsive potential, determined by the application of Gilbert–Smith combining rules,[12(c)] plus an attractive potential with dispersion terms estimated using precise combining rules.[12(b)] The expression for the TT potential is ($n=0,2$)

$$V_n = V_{\mathrm{SCF}n} - V_{\mathrm{disp}n} + V_{\mathrm{corr}n} , \tag{A1}$$

where V_{SCF} is the SCF repulsive energy, V_{disp} is the dispersion energy, and V_{corr} is the coupling correction. The individual terms in Eq. (A1) are modeled by the following analytic forms[12(c),21]:

$$V_{\mathrm{SCF0}} = \tfrac{1}{3}(V_{\mathrm{SCF}\parallel} + 2V_{\mathrm{SCF}\perp}) , \quad V_{\mathrm{corr0}} = \tfrac{1}{3}(V_{\mathrm{corr}\parallel} + 2V_{\mathrm{corr}\perp}) ,$$

$$V_{\mathrm{SCF2}} = \tfrac{2}{3}(V_{\mathrm{SCF}\parallel} - V_{\mathrm{SCF}\perp}) , \quad V_{\mathrm{corr2}} = \tfrac{2}{3}(V_{\mathrm{corr}\parallel} - V_{\mathrm{corr}\perp}) ,$$

and

$$V_{\mathrm{SCF}\parallel,\perp} = A_{\parallel,\perp} \exp(-b_{\parallel,\perp} R) ,$$

$$V_{\mathrm{corr}\parallel,\perp} = [M(\mathrm{H_2})_{\parallel,\perp} + M(\mathrm{Ar})] \times (b^2_{\parallel,\perp} - 2b_{\parallel,\perp}/R) \cdot A_{\parallel,\perp} \exp(-b_{\parallel,\perp} R) ,$$

$$V_{\mathrm{disp0}} = C_6 R^{-6} , \qquad R \leqq R_{3,4} ,$$

$$V_{\mathrm{disp0}} = \sum_{n=3}^{n'-1} C_{2n} R^{-2n} + f_{2n'} C_{2n'} R^{-2n'} , \qquad R_{n'-1,n'} \leqq R \leqq R_{n',n'+1} ,$$

$$V_{\mathrm{disp0}} = \sum_{n=3}^{11} C_{2n} R^{-2n} , \qquad R \geqq R_{11,12} ,$$

where n' in succession equals 4, 5, 6, 7, 8, 9, 10, and 11, and

$$f_{2n'} = (R - R_{n'-1,n'})/(R_{n',n'+1} - R_{n'-1,n'}) ,$$

$$V_{\mathrm{disp2}} = \Gamma_6 C_6 R^{-6} , \qquad R \leqq R_{3,4} ,$$

$$V_{\mathrm{disp2}} = \Gamma_6 C_6 R^{-6} + \Gamma_8 f_8 C_8 R^{-8} , \qquad R_{3,4} \leqq R \leqq R_{4,5} ,$$

$$V_{\mathrm{disp2}} = \Gamma_6 C_6 R^{-6} + \Gamma_8 C_8 R^{-8} + \Gamma_{10} f_{10} C_{10} R^{-10} , \qquad R_{4,5} \leqq R \leqq R_{5,6} ,$$

$$V_{\mathrm{disp2}} = \Gamma_6 C_6 R^{-6} + \Gamma_8 C_8 R^{-8} + \Gamma_{10} \times \left(\sum_{n=5}^{n'-1} C_{2n} R^{-2n} + f_{2n'} C_{2n'} R^{-2n'} \right) , \qquad R_{n'-1,n'} \leqq R \leqq R_{n',n'+1} ,$$

$$V_{\mathrm{disp2}} = \Gamma_6 C_6 R^{-6} + \Gamma_8 C_8 R^{-8} + \Gamma_{10} \sum_{n=5}^{11} C_{2n} R^{-2n} , \qquad R \geqq R_{11,12} ,$$

where n' in succession equals 6, 7, 8, 9, 10, and 11. The dispersion coefficients can be obtained with the recursion relation $C_{2n+6} = (C_{2n+4}/C_{2n+2})^3 C_{2n}$ and the boundaries $R_{n,n+1}$ are obtained from the ratios of dispersion coefficients $R_{n,n+1} = (C_{2n+2}/C_{2n})^{1/2}$. The molecular parameters of the TT potential for the Ar···H_2 system are listed in Table III and the potential curves are shown in Fig. 1(e).

[1]For a recent review, see R. J. Le Roy and J. S. Carley, Adv. Chem. Phys. **42**, 353 (1980).
[2]For recent reviews, see (a) J. Reuss, Adv. Chem. Phys. **30**, 389 (1976); (b) K. Thuis, S. Stolte, and J. Reuss, Comments At. Mol. Phys. **8**, 123 (1979).
[3](a) L. Zandee and J. Reuss, Chem. Phys. **26**, 327 (1977); (b) **26**, 345 (1977).
[4](a) R. J. Le Roy and J. van Kranendonk, J. Chem. Phys. **61**, 4750 (1974); (b) R. J. Le Roy, J. S. Carley, and J. E. Grabenstetter, Faraday Discuss. Chem. Soc. **62**, 169 (1977); (c) J. S. Carley, *ibid.* **62**, 303 (1977); (d) J. S. Carley, Ph. D. thesis, University of Waterloo, Waterloo, Ontario, 1978.
[5]A. M. Dunker and R. G. Gordon, J. Chem. Phys. **68**, 700 (1978).
[6]K. E. Johnson, L. Wharton, and D. H. Levy, J. Chem. Phys. **69**, 2719 (1978), and references cited therein; T. E. Gough, R. E. Miller, and G. Scoles, *ibid.* **69**, 1588 (1978).
[7]J. E. Grabenstetter and R. J. Le Roy, Chem. Phys. **42**, 41 (1979).
[8]J. A. Beswick and A. Requena, J. Chem. Phys. **73**, 4347 (1980).
[9]S.-I Chu, J. Chem. Phys. **72**, 4772 (1980).
[10]See, for example, Int. J. Quantum Chem. **14**, No. 4 (1978).
[11](a) Z. Bacic and J. Simons, Int. J. Quantum Chem. **14**, 467 (1980); (b) O. Atabek and R. Lefebvre, Chem. Phys. **55**, 395 (1981).
[12](a) K. T. Tang and J. P. Toennies, J. Chem. Phys. **66**, 1496 (1977); (b) **68**, 5501 (1978); (c) **74**, 1148 (1981).
[13]A. M. Arthurs and A. Dalgarno, Proc. R. Soc. London Ser. A **256**, 540 (1960).
[14]E. Balslev and J. M. Combes, Commun. Math Phys. **22**, 280 (1971); J. Aguilar and J. M. Combes, *ibid.* **22**, 265 (1971); B. Simon, *ibid.* **27**, 1 (1972); Ann. Math. **97**, 247 (1973).
[15]I. C. Percival and M. J. Seaton, Proc. Cambridge Philos. Soc. **53**, 654 (1957).
[16]J. P. Toennies, W. Welz, and G. Wolf, J. Chem. Phys. **71**, 614 (1979).
[17]R. Helbing, W. Gaide, and H. Pauly, Z. Phys. **208**, 215 (1968).
[18]C. S. Lin and G. W. F. Drake, Chem. Phys. Lett. **16**, 35 (1972).
[19]Since only one complex eigenvalue is desired, the inverse iteration technique (see, for example, Ref. 20) was used, which reduced the amount of computer time substantially.
[20]S.-I Chu, Chem. Phys. Lett. **54**, 367 (1978).
[21]M. Waaijer, Ph. D. thesis, Katholieke University, Nijmegen, The Netherlands, 1981.
[22]A. M. Rulis, K. M. Smith, and G. Scoles, Can. J. Phys. **56**, 753 (1978).
[23]The spurious widths associated with the unperturbed van der Waals vibrational bound states occur because the diagonal-block matrices such as $\langle j=l=2, n \mid H_\alpha \mid j'=l'=2, n' \rangle$ are complex symmetric. In general, a smaller spurious width indicates a better quality of the bound state wave function. The (real) physical widths are induced by the off-diagonal coupling blocks.
[24]K. K. Datta and S.-I. Chu, Scaling, Chem. Phys. Lett. (in press).
[25]K. K. Datta and S.-I Chu (to be published).
[26]S.-I. Chu and K. K. Datta (to be published).
[27](a) B. Schneider, Chem. Phys. Lett. **31**, 237 (1975); (b) T. N. Rescigno, C. W. McCurdy, Jr., and A. E. Orel, Phys. Rev. A **17**, 1931 (1978).
[28]D. O. Harris, G. C. Engerholm, and W. D. Gwinn, J. Chem. Phys. **43**, 1515 (1965).
[29]The kinetic energy matrix elements are independent of the coordinate (X or R) used for complex rotation.
[30]S.-I Chu (unpublished results).
[31]The fact that the spurious widths of the BC and TT potentials do not decrease rapidly with N is probably mainly due to the inhomogeneity or piecewise nature of their analytic representations.
[32]The strength of the anisotropy is best measured by the magnitude of the anisotropic parameters such as q_6 and q_{12} of LJ potentials in Table I. It is seen there that LJ(I) has the largest q_6 and q_{12} values and, therefore, is the "strongest" anisotropic potential.
[33]Although the spread of the linewidths (Γ) for the various potentials (Fig. 9) are mainly caused by the differences among the anisotropic potentials, the spread of the resonance energies (E_R) can be largely accounted for (within 90%) by the differences among the zero-order isotropic potentials.
[34]K. P. Huber and G. Herzberg, *Molecular Spectra and Molecular Structure* (Van Nostrand Reinhold, New York, 1979), Vol. IV.